

1 **The curious case of a strong relationship between**
2 **ENSO and Indian summer monsoon in CFSv2 model**

3 **Priyanshi Singhai^{1,2}, Arindam Chakraborty^{1,2,3}, Kaushik Jana⁴, Kavirajan**
4 **Rajendran⁵ and Sajani Surendran⁵**

5 ¹Centre for Atmospheric and Oceanic Sciences, Indian Institute of Science, Bengaluru, 560012, India

6 ²Divecha Centre for Climate Change, Indian Institute of Science, Bengaluru, 560012, India

7 ³DST-Centre of Excellence in Climate Change, Divecha Centre for Climate Change, Indian Institute of
8 Science, Bengaluru 560012, India.

9 ⁴Mathematical and Physical Sciences Division, Ahmedabad University, Ahmedabad-380009, India

10 ⁵CSIR Fourth Paradigm Institute (CSIR-4PI), Bangalore-560037, India

11 **Key Points:**

- 12 • In CFSv2, the consensus on ENSO forcing sign among ensemble members effectively
13 represents ENSO's influence in the ensemble mean.
- 14 • Non-ENSO climate forcings, despite being present in individual members, vary con-
15 siderably, attenuating non-ENSO signals in the ensemble mean.
- 16 • Hence, the ensemble mean shows a strong ENSO-ISMR correlation, while individual
17 ensemble members do not exhibit the same relationship.

Corresponding author: Priyanshi Singhai, priyanshis@iisc.ac.in, pspriyanshi66@gmail.com

Abstract

18 **Abstract**
19 An ensemble of forecasts is necessary to identify the uncertainty in predicting a non-linear
20 system like climate. While ensemble averages are often used to represent the mean state and
21 diagnose physical mechanisms, they can lead to information loss and inaccurate assessment
22 of the model's characteristics. We highlight an intriguing case in the seasonal hindcasts of
23 the Climate Forecast System version-2. While all ensemble members often agree on the sign
24 of predicted El Nino Southern Oscillation (ENSO) for a particular season, non-ENSO climate
25 forcings, although present in individual members, are disparate. As a result, an ensemble
26 mean retains ENSO anomalies while diminishing non-ENSO signals. This difference between
27 ENSO and non-ENSO predictions and a more decisive impact of ENSO on seasonal climate
28 increases the ensemble mean ENSO-Indian Summer Monsoon Rainfall correlation. Thus,
29 a model's teleconnection skills, which often help interpret physical mechanisms, should be
30 studied using individual members rather than ensemble averages.

Plain Language Summary

31 **Plain Language Summary**
32 When it comes to predicting a chaotic system like climate, we generate a set of fore-
33 casts known as an ensemble. Each forecast in the ensemble starts from slightly different
34 initial conditions. To evaluate the performance of the climate model, we often calculate the
35 average of the ensemble. But only looking at the ensemble average can sometimes over-
36 look important information and make our evaluations of the climate model less accurate.
37 Here, we presented one such example where the ensemble mean fails to represent the true
38 characteristic of the model. Previous studies reported that the year-to-year variations of
39 the Indian summer monsoon rainfall in many climate models are heavily influenced by the
40 climate of the central and eastern Pacific oceans. However, our analysis reveals that this
41 relationship stems from the methodology used to compute ensemble mean rather than be-
42 ing an inherent characteristic of the model. Hence, our study highlights the importance of
43 examining individual ensemble members to evaluate the models' forecasting abilities.

1 Introduction

Ensemble forecasting has become widely adopted for predicting inherently chaotic and non-linear systems like weather and climate (Molteni et al., 1996; Palmer, 2000). This approach involves running a numerical prediction model multiple times with different initial conditions or numerical atmospheric representations to address forecast uncertainty (Palmer, 2000; Leutbecher & Palmer, 2008; Weisheimer et al., 2011). Moreover, ensemble averages of forecasts are commonly used to address systematic model errors and represent forecasts as anomalies. This approach relies on the forecast value for a specific start time, lead time, and target period. However, there can be challenges if a forecast ensemble mean is needed for start times that are not included in the hindcasts or if the number of hindcasts is considerably smaller than the variance of the forecast anomaly (Tippett et al., 2018). Despite these challenges, numerous studies have extensively utilized this method to evaluate the model's teleconnection patterns and forecast skill in simulating Indian summer monsoon rainfall (ISMR).

The year-to-year variation of ISMR is primarily influenced by low-frequency variations in tropical sea surface temperatures (Charney & Shukla, 1981), particularly El Nino Southern Oscillation (ENSO) (Rasmusson & Carpenter, 1983; J. Shukla & Wallace, 1983). However, the impact of these SST variations on monsoons can vary due to the inherent chaotic nature of the climate system. Hence, the generation of ensemble forecasts becomes imperative to estimate the uncertainty associated with the ISMR predictions and to evaluate the model performance in predicting monsoons. Many of the climate models like ECMWF-SYSTEM4, North American Multi-Model Intercomparison Project (NMME), and CMIP models heavily rely on ENSO for ISMR prediction (Kim et al., 2012; Pillai et al., 2021; He et al., 2022; Rajendran et al., 2022). Interestingly, some models exhibit an ENSO-ISMR relationship that is nearly twice as strong as observed (Singh et al., 2019). For example, many coupled models of CMIP5 show a similar strong association, which attributes it to the westward shift of the anomalous low-level anticyclonic circulation over the tropical Indian

71 Ocean and western subtropical northwest Pacific. This shift causes an advection of dry
72 air from the extratropics to the Indian region, causing a stronger ENSO-ISMR relationship
73 (Ramu et al., 2018). The NCEP Climate Forecast system version-2 (CFSv2) model also
74 demonstrates an overestimation of this relationship (George et al., 2016; Chattopadhyay et
75 al., 2016), potentially due to an underestimation of synoptic activity over the Bay of Bengal
76 in August, which amplifies the impact of ENSO on ISMR in the model (Das et al., 2022).
77 Furthermore, the ENSO-ISMR relationship in the CFSv2 might also be influenced by SST
78 biases in the equatorial central Pacific and Indian oceans (R. P. Shukla & Huang, 2016).
79 Another study highlighted that the observed fluctuation in the ENSO-ISMR correlation over
80 a longer period could also be ascribed to sampling variability (Cash et al., 2017; Gershunov
81 et al., 2001). This finding is shown using a large ECMWF Ensemble Prediction System
82 ensemble. Several studies also examine the impact of another variability on ISMR in the
83 CFSv2. One of these studies suggests that the model has a problem capturing the air-sea in-
84 teraction over the Indian Ocean and low-level winds over the Indian region (Krishnamurthy,
85 2018). Additionally, another study by (Sabeerali et al., 2019) indicates that CFSv2 has poor
86 predictive skills in forecasting the teleconnection between the Atlantic zonal mode and ISM.

87 Although the above studies analyzed the model's teleconnection patterns using the
88 ensemble average of the forecast, relying solely on this approach could lead to the loss
89 of valuable information embedded within the individual ensemble forecasts. Hence, our
90 objective is to investigate whether the ensemble mean of the forecasts reflects the true
91 behavior of the model or displays distinct characteristics when compared to the individual
92 ensemble members. We also want to ascertain whether the model errors discussed earlier
93 are a consequence of inherent limitations in the model or are influenced by the methodology
94 employed to analyze the teleconnection patterns.

2 Model Description, Experimental Design, and Observational Data sets

We utilize the National Centers for Environmental Prediction (NCEP) CFSv2 model, which is fully coupled and includes the NCEP GFS (Global forecast system) for the atmospheric component, Geophysical Fluid Dynamics Laboratory Modular Ocean Model version 4 for the ocean model, a two-layer sea ice model, and a four-layer Noah land surface model (Saha et al., 2014). GFS has a horizontal resolution of 0.91° and 64 vertical levels. The model simulation is performed at the computing platform of Council for Scientific and Industrial Research (CSIR) Fourth Paradigm Institute, Bengaluru, following the experimental setup used by Rajendran et al. (2021) and Singhai et al. (2023). The model is integrated for nine months using five different initial conditions for the period of 1979–2016. The initial conditions include 00UTC of 21 April (member 1), 26 April (member 2), 1 May (member 3), 6 May (member 4), and 11 May (member 5). This is referred to as “Model 1” or M1 in this study. Additionally, to verify the M1 results, the study also analyzes 124 nine months of reforecast (referred to as “Model 2” or M2) initialized from CFS-based initial conditions every fifth day from 1 January to 31 May, with four reforecasts per day (00, 06, 12, 18 UTC) from 1982 to 2010 (Saha et al., 2010).

The objective of this study is to investigate the difference in the model’s characteristics in individual ensemble members and their mean. We treat each of the initial conditions reforecasts as a distinct entity to obtain the characteristic of individual members (E_{all}). Conversely, we calculate the ensemble mean using the following approach:

By assuming the linear superposition of different forcings, such as ENSO, IOD, and ATL, on ISMR, we can express ISMR (P) as follows:

$$P = C_0 + \sum_{j=1}^n C_j f_j \quad (1)$$

where f_j is the j^{th} forcing and C_j are constants. The term C_0 can be neglected with the removal of the climatological values.

120 If there are m members of an ensemble prediction system, the above equation applies
 121 separately to each of the ensemble members. Thus, the ensemble mean (E_M) for ISMR can
 122 be computed in the following way.

$$123 \quad \bar{P} = \sum_{j=1}^n C_j \bar{f}_j \quad (2)$$

124 Here, C_j remains unchanged as it represents the model's characteristics, while \bar{f}_j represents
 125 the ensemble mean forcing and is computed by averaging the values across each ensemble
 126 member, as shown below.

$$127 \quad \bar{f}_j = \frac{1}{m} \sum_{i=1}^m f_i$$

128 For model validation against observations, we use the June-September (JJAS) averaged
 129 Extended reconstructed sea surface temperature (ER-SST) version 5 data to derive the
 130 ENSO index (Huang et al., 2017). The India Meteorological Department (IMD) monthly
 131 mean gridded rainfall dataset with a spatial resolution of $1^\circ \times 1^\circ$ is used to calculate ISMR
 132 (Rajeevan et al., 2006). JJAS average GPCP (Global Precipitation Climatology Project)
 133 data is also utilized to depict changes in precipitation over land and ocean (Huffman et al.,
 134 2009).

135 **Index calculation**

136 The area-averaged rainfall over the region (7.5° – 27.5° N, 70° – 90° E) during the boreal
 137 summer monsoon season is used to define ISMR (Parthasarathy et al., 1994). For ISMR
 138 computation, only land grid points are considered. The ENSO index is the area-average
 139 SST anomaly over the Nino 3.4 region (5° S– 5° N, 170° W– 120° W). SST anomaly greater
 140 (less) than 0.5° C (-0.5° C) is classified as El Nino (La Nina). The ATL is defined as the
 141 averaged SST anomaly over a region (20° S–Eq, 30° W– 20° E) (Kucharski et al., 2008, 2007).
 142 The positive (negative) phases of ATL are identified when the JJAS averaged values exceed
 143 one (less than minus one) standard deviation.

144 Likelihood histogram

145 The likelihood histogram displays the distribution of ensemble members exhibiting co-
 146 herent behavior, with a threshold of 0°C for both the ENSO and ATL indices. For a partic-
 147 ular year, we determine the maximum number of ensemble members showing the same sign
 148 of anomaly (>0 or <0). For instance, years where all five ensemble members showed either
 149 a positive or negative ENSO index, are grouped in bin 5, while the 4 and 3 contained years
 150 with fewer coherent members.

151 3 Results

152 ENSO has a strong relationship with ISMR, with a correlation coefficient of -0.58 , as
 153 shown in Fig 1a. However, the majority of the climate models, including CFSv2, overes-
 154 timate the impact of ENSO on boreal summer monsoon rainfall, as reported in previous
 155 studies (Kim et al., 2012; R. P. Shukla & Huang, 2016; He et al., 2022; Rajendran et al.,
 156 2022). These studies often use the ensemble average method to examine the teleconnec-
 157 tion patterns in the seasonal and sub-seasonal prediction systems. Although this method
 158 effectively reduces the random variations or “noise” inherent in ensemble forecasts, it also
 159 results in the loss of important information. For instance, Figure 1a depicts the relationship
 160 between ENSO and ISMR for the CFSv2 models 1 (M1) and 2 (M2). This association is
 161 shown using both individual (E_{all} , yellow bars) and the mean of ensemble members (E_M ,
 162 red bars). It should be noted that there is a significant difference in the ENSO-ISMV rela-
 163 tionship computed from these two methods for both M1 and M2. The correlation coefficient
 164 (CC) for the E_{all} ($CC_{M1} = -0.55$ and $CC_{M2} = -0.58$) is comparable to that seen in the ob-
 165 servation ($CC = -0.58$). However, the relationship is greatly overestimated for E_M , resulting
 166 in a high correlation coefficient of -0.7 (M1) and -0.88 (M2). Furthermore, despite model
 167 M2 having a significantly larger number of ensemble members compared to model M1, there
 168 is a greater disparity in the correlation coefficient between E_M and E_{all} for M2 than for
 169 M1. This suggests that the strong relationship between ENSO and ISMR in the CFSv2

170 model, as reported by previous literature, is not a characteristic inherent to the model but
 171 stems from the ensemble average method. In addition, it is worth noting that our primary
 172 finding remains robust and consistent regardless of the number of ensemble members used
 173 in models M1 and M2. This highlights the reliability of our results, despite the potential
 174 impact of the number of ensemble members on the efficacy of the ensemble average method
 175 (Atger, 1999).

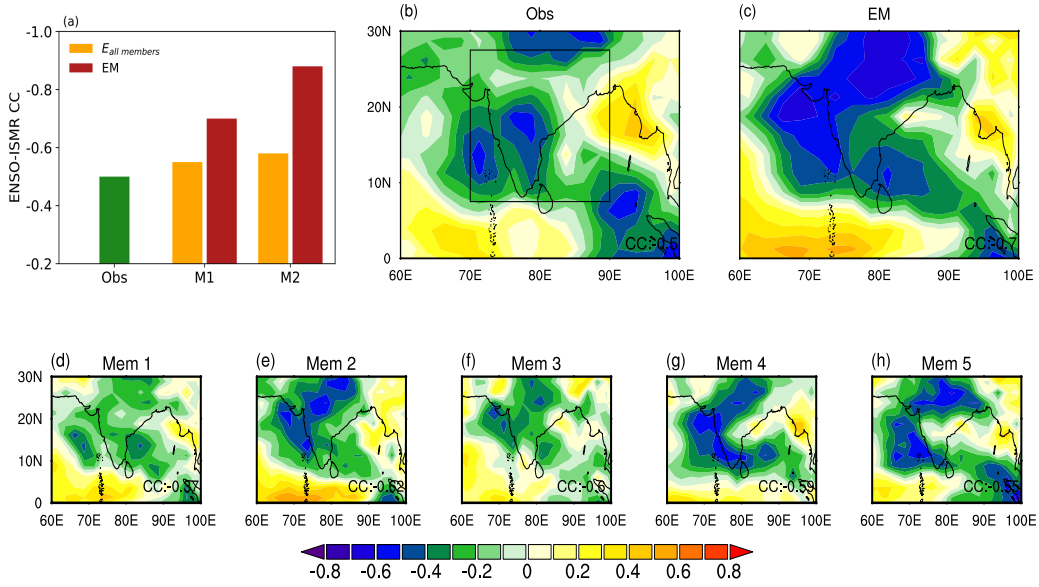


Figure 1. (a) The bar plot illustrates the relationship between ENSO and ISMR for the observation, as well as the CFSv2 models M1 (with 5 ensemble members) and M2 (with 124 ensemble members). This relationship is depicted using both individual members (E_{all}) and the ensemble mean (E_M) of the CFSv2 seasonal hindcasts. (b-h) The spatial composite of the correlation coefficient between the ENSO index and precipitation over the South Asian region. Panel (b) represents the observation, panel (c) shows the ensemble mean (E_M), and panels (d-h) present the correlation for all five individual ensemble members of model M1 (21 April (Mem 1), 26 April (Mem 2), 1 May (Mem 3), 6 May (Mem 4), and 11 May (Mem 5)). The inset value in (b-h) is for the correlation coefficient (CC) between ISMR and ENSO index for 1979-2016.

176 Figure 1b-h displays the spatial patterns showing the response of ENSO to ISMR for
 177 observation (Fig. 1b), ensemble mean (Fig. 1c), and the individual ensemble members (Fig.
 178 1d-h) of model M1. Negative values of the correlation coefficient mark the entire Indian
 179 region in all three cases. However, these values are significantly higher for the ensemble mean

180 than for observation and other ensemble members. The negative values in the ensemble
 181 mean mainly concentrate on the western ghats and northern parts of the Indian region,
 182 particularly over the Indo-Gangetic belt (Fig 1c). The reason for such high negative values
 183 in the ensemble mean can be understood by examining the behavior of individual ensemble
 184 members. It is worth noting that the response of ENSO to ISMR varies significantly among
 185 ensemble members, ranging from -0.37 to -0.62 . Member 1 displays the weakest ENSO
 186 response to ISMR with a CC of -0.37 . In contrast, other members show a considerably
 187 strong relationship, albeit weaker than the ensemble mean. In addition, the negative CC
 188 among the ensembles, particularly for members 2, 4, and 5, are heterogeneously clustered
 189 over northern India. As a result, when the ensemble average is computed, the negative
 190 values are superimposed in a manner that causes the ENSO-ISMIR relationship to be higher
 191 in the ensemble mean than in the individual members.

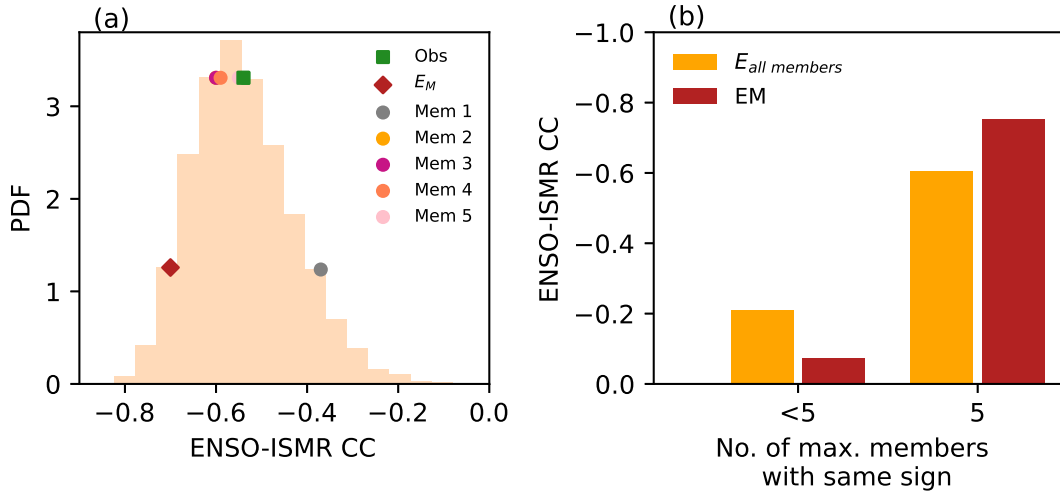


Figure 2. (a) The probability density function (PDF) of the correlation coefficient (CC) between ENSO forcing and Indian summer monsoon rainfall (ISMIR). This analysis is based on a 38-year sample extracted from a total of 190 individual ensemble members. This process is randomized and repeated over 1000 iterations. Additionally, the CC values for the observation, the ensemble mean, and all five individual ensemble members (21 April (Mem 1), 26 April (Mem 2), 1 May (Mem 3), 6 May (Mem 4), and 11 May (Mem 5)) for the period of 1979–2016 are also indicated as markers. (b) The bar plot shows the ENSO-ISMIR relationship when all 5 and less than 5 ensemble members exhibit the same sign of ENSO anomalies. The year distribution of the cases where there are 5 and <5 members having the same sign of ENSO anomalies are shown in Figure 3.

192 Figure 2a shows the probability distribution of the potential ENSO-ISMR correlation
 193 coefficients, generated by randomly selecting 38 years from the ensemble forecast of 190
 194 years (38 years \times five initial conditions). This process is randomized and repeated over 1000
 195 times. Interestingly, the maximum likelihood of getting the correlation coefficient between
 196 ENSO-ISMR is -0.55 (mode), which is similar to the correlation corresponding to the
 197 observation and individual ensemble members. Additionally, four out of the five ensemble
 198 members are clustered around the mode value. The probability of getting the correlation
 199 coefficient of the ensemble mean ($CC=-0.7$) is much lower than that of CC computed
 200 using individual ensemble members ($CC=-0.55$). Once again, this finding confirms that
 201 the strong relationship between ENSO and ISMR observed in E_M is not an intrinsic feature
 202 of the CFSv2 model.

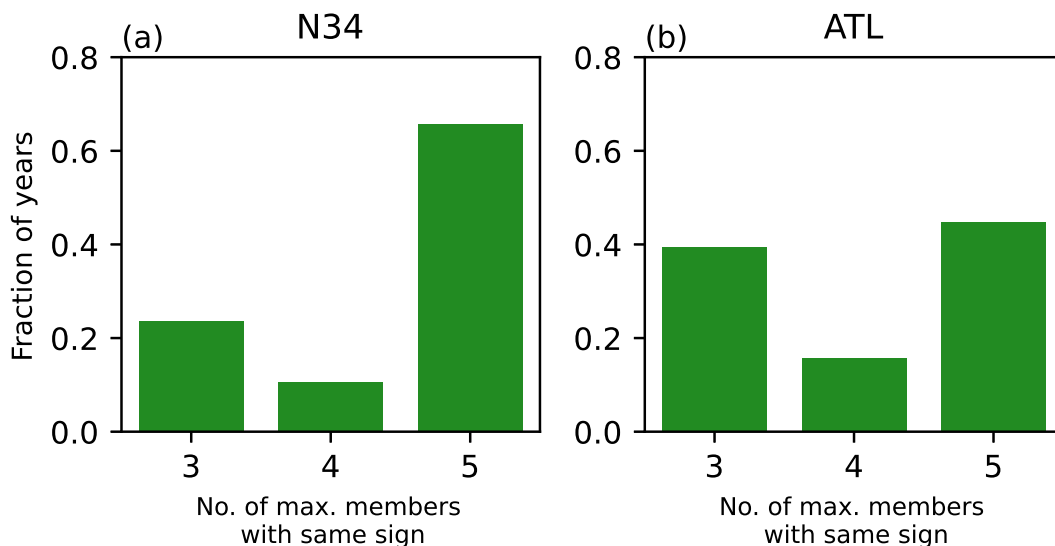


Figure 3. The histograms show the distribution of the maximum number of ensemble members exhibiting the same signs of an anomaly for (a) ENSO Index (N34) and (b) Atlantic tropical variability (ATL).

203 To investigate the differing response of ENSO on ISMR between the ensemble mean and
 204 individual ensemble members, we generate a histogram in Figure 3a to examine the behavior
 205 of each individual member under ENSO forcing. Additionally, since external forcings such
 206 as ATL can suppress the influence of ENSO on ISMR (Kucharski et al., 2008), the histogram

207 for ATL is also shown in Fig 3b. Our analysis shows that there is a high probability (around
208 66%) of obtaining the same sign of anomaly (either $N34 > 0$ or $N34 < 0$) by all five ensembles
209 under ENSO forcing. Our analysis shows that there is a high probability (around 66%) of
210 obtaining the same signs of anomaly (either $N34 > 0$ or $N34 < 0$) for each year across all five
211 ensemble members under ENSO forcing. This leads to the ENSO forcing dominating the
212 ensemble mean over individual members. As a result, the ENSO-ISMR relationship in the
213 ensemble mean is majorly determined by these five coherent members ($CC_5 = -0.77$, Figure
214 2c). This leads to the retainment of the ENSO forcing in the ensemble mean, leading to a
215 pronounced ENSO-ISMR relationship. This relationship in the ensemble mean is majorly
216 determined by the years where all five ensemble members exhibit the coherent anomaly
217 signs ($CC_5 = -0.77$, Figure 2c). In contrast, the contribution of members showing incoherent
218 behavior (< 5) is negligible ($CC_{<5} = -0.08$, Figure 2b). Notably, we also observe that the
219 ENSO-ISMR relationship derived from the ensemble mean of the incoherent member (< 5)
220 is weaker than that computed from individual members (Fig 2b). This can be due to the
221 cancellation of the ENSO forcing caused by the varying responses of ENSO among different
222 ensemble members. On the other hand, for non-ENSO forcing, such as ATL, the likelihood
223 of all five ensemble members exhibiting the same sign is much lower than ENSO forcing
224 (Fig 3b). This may be due to non-linear processes over the Atlantic Oceans, contributing to
225 the model's differing behavior among ensembles. Hence, in the case of non-ENSO forcing,
226 even though it exists in individual members, it shows significant variability, resulting in the
227 weakening of non-ENSO signals in the ensemble mean.

228 External climatic forcings such as ENSO and ATL tend to perturb the surface pres-
229 sure patterns surrounding the Indian region, leading to modifications in the incoming and
230 outgoing moisture fluxes (Chakraborty & Singhai, 2021). These fluxes, primarily from the
231 Arabian Sea (F_W) and the Bay of Bengal (F_E), play a vital role in driving atmospheric
232 convection over India during the boreal summer monsoon. Figure 4 shows a scatter plot
233 that facilitates the examination of potential disparities in the responses of ENSO and ATL
234 to moisture fluxes between individual members and the ensemble mean. To accomplish this,

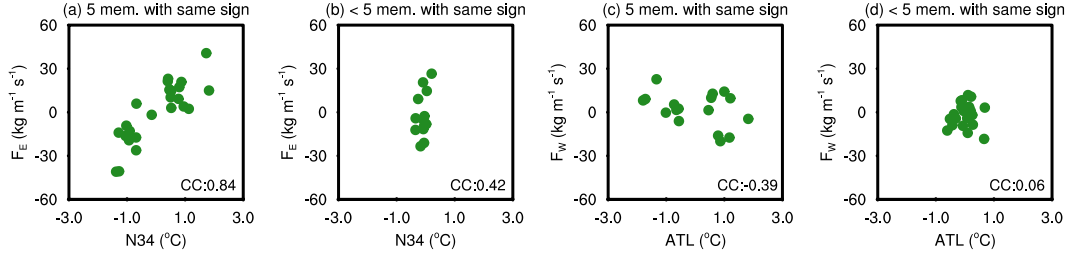


Figure 4. The scatter plots show the relationship between the ENSO index and moisture flux over the Bay of Bengal (F_E) when there is a maximum of (a) five and (b) less than five ensemble members with the same signs of ENSO anomaly. Similarly, in plots (c, d), we examine the relationship between ATL forcing and moisture flux over the Arabian Sea (F_W) for these two cases. To quantify the impact of ATL, we regress out the impact of ENSO from total moisture fluxes (explained in Supplementary Note 1).

235 we focus on dominant moisture fluxes such as F_E , which plays a crucial role in regulating
 236 ENSO-driven rainfall in the model (Supplementary Figure 1), also shown by Singhai et al.
 237 (2023) through analysis of individual ensemble members. Additionally, we examine the role
 238 of F_W , the primary factor driving rainfall during ATL events (Supplementary Figure 2).
 239 We then segregate the forcing and moisture fluxes based on years where five and less than
 240 five members show the same sign of forcings (same way as in Figure 3). We notice that the
 241 correlation between ENSO and F_E is higher in years when all members are coherent in sign
 242 (CC=0.84) than in fewer coherent members (CC=0.42). Hence, the impact of F_E on the
 243 ensemble mean is maintained when all members exhibit consistent signs, while its influence
 244 diminishes when there are fewer members with coherent signs. Furthermore, as depicted in
 245 Figure 4b, it is evident that the variability of ENSO forcing is significantly reduced when
 246 fewer than five ensemble members exhibit the same sign, in contrast to the case when all
 247 five members have coherent signs. It is due to the opposite signs of ENSO forcing in the in-
 248 dividual ensemble members, which tend to cancel out each other, resulting in the decreased
 249 variability of ENSO in the <5 case. As depicted in Figure 3b, the number of members
 250 with coherent signs is lower for ATL than for ENSO. As a result, the impact of ATL in
 251 the ensemble mean is reduced compared to ENSO. This reduction in ATL forcing leads to
 252 a weaker response, as shown in Fig 4c and 4d. Moreover, similar to ENSO, the impact of

253 ATL forcing on F_W is more pronounced when all members have the same anomaly sign, as
 254 opposed to when there are fewer coherent sign members. This emphasizes that disparity in
 255 the impact of ENSO and ATL forcing on moisture fluxes between the ensemble mean and
 256 individual ensemble members is primarily influenced by the maximum number of ensemble
 257 members exhibiting a consistent sign of forcing.

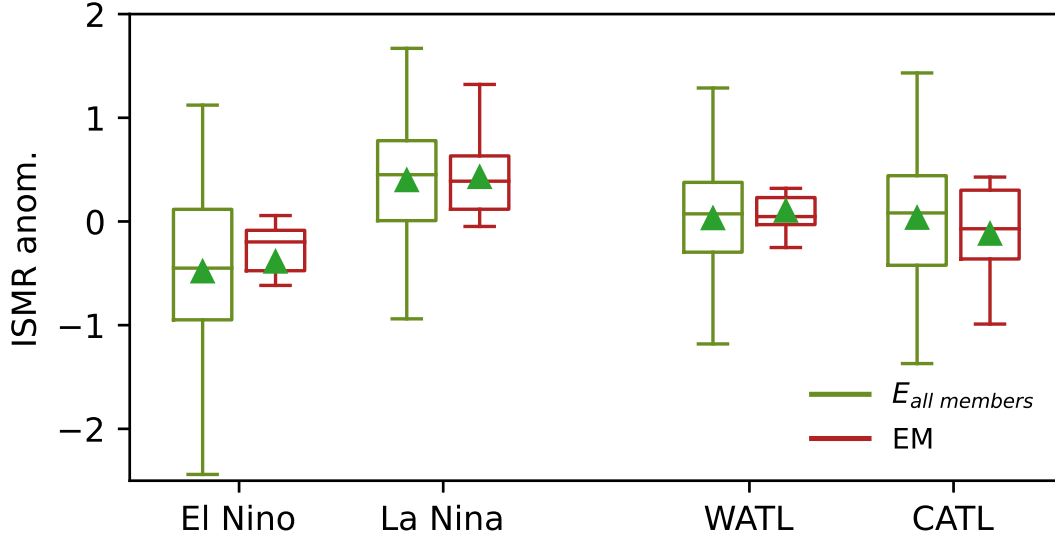


Figure 5. The box plot shows the ISMR response to positive and negative phases of ENSO (El Nino and La Nina) and ATL (Warm-ATL and Cold ATL) forcing.

258 Figure 5 illustrates the response of rainfall to positive and negative phases of ENSO
 259 and ATL in both the ensemble mean and individual ensemble members. The relationship
 260 between El Nino (La Nina) events and ISMR is observed to be different in the ensemble
 261 mean compared to the individual members, with almost all El Nino (La Nina) events leading
 262 to a decrease (increase) in ISMR in the former, but this is not the case in the latter. This
 263 difference is attributed to the high ENSO-ISMR relationship observed in the ensemble mean,
 264 which is a result of a maximum number of members exhibiting the coherent sign (as shown
 265 in Figure 3a). This finding also suggests that the model simulates the mean response of
 266 positive and negative ENSO phases to ISMR correctly. This response is largely governed
 267 by the climate of the Bay of Bengal (Singhai et al. (2023), Figure 4a). Conversely, similar
 268 to ENSO events, the rainfall variability sharply decreases in the ensemble mean compared

269 to the individual ensemble member during ATL events. This could be attributed to the
270 suppressed effect of ATL forcing due to the negation of forcing caused by members having
271 opposite anomaly signs. To summarize, the stronger relationship between ENSO and ISMR
272 observed in the ensemble mean is primarily influenced by the agreement among ensemble
273 members with the same ENSO anomaly sign. Nevertheless, the non-ENSO climate forcings
274 present in individual members display substantial variability, leading to a reduction in the
275 strength of non-ENSO signals within the ensemble mean.

276 **4 Summary and discussions**

277 The primary aim of this study is to address the critical issue of imprudent usage of
278 the ensemble mean approach for evaluating the forecasting skills of climate models. It is
279 observed that relying solely on the ensemble mean method neglects the valuable information
280 embedded within individual ensemble members, potentially leading to erroneous evaluations
281 of the model's teleconnection patterns. Our study highlights a notable case of a strong
282 ENSO-ISMR relationship in the CFSv2 seasonal hindcasts. Previous studies have reported
283 that the CFSv2 model, like many other climate forecast models, is subject to the strong
284 influence of ENSO on ISMR (Kim et al., 2012; R. P. Shukla & Huang, 2016; He et al.,
285 2022; Rajendran et al., 2022). Our analysis, however, suggests that this pronounced ENSO-
286 ISMR relationship is primarily observed in the ensemble mean, while it is not apparent in
287 the individual ensemble members. Hence, we aim to discern the underlying mechanisms
288 contributing to the distinctive response of ENSO to ISMR in the ensemble mean versus
289 individual ensemble members.

290 This observed discrepancy between the ensemble mean and individual ensemble mem-
291 bers attributes to a change in the nature of forcing and its associated response during the
292 computation of the ensemble mean. In particular, the strong relationship between ENSO
293 and ISMR observe in the ensemble mean primarily stems from the consensus among en-
294 semble members regarding the sign of ENSO anomaly. This retains the influence of ENSO

295 in the ensemble mean. Conversely, the significant variability of the non-ENSO forcings in
296 individual members diminishes the strength of non-ENSO signals within the ensemble mean.

297 Our study highlights the significance of examining individual ensemble members rather
298 than solely relying on the ensemble mean in order to gain a comprehensive understanding
299 of a climate model's characteristics and forecasting abilities. Specifically, we find that the
300 prevalent issue of a strong ENSO-ISMR relationship in many climates models may not
301 necessarily stem from a fundamental lacuna within the model but rather arises from the
302 methodology employed in calculating the ensemble mean.

303 **Acknowledgments**

304 AC, KR, and SS acknowledge the National Monsoon Mission funded by the Ministry of
305 Earth Sciences (MoES), Government of India for supporting the research. The authors
306 thank IMD and NOAA for providing rainfall and SST data sets, respectively. We thank
307 the computing platform of the Council for Scientific and Industrial Research (CSIR) Fourth
308 Paradigm Institute, Bengaluru for carrying out the CFSv2 simulations. We are also thankful
309 to NCEP for making CFSv2 retrospective runs available.

310 **5 Open Research**

311 **Data availability**

312 The rainfall data utilized in the study are obtained from the IMD ([https://impune](https://impune.gov.in/ndc_new/Request.html)
313 [.gov.in/ndc_new/Request.html](https://impune.gov.in/ndc_new/Request.html)) and GPCP ([https://ps1.noaa.gov/data/gridded/data](https://ps1.noaa.gov/data/gridded/data.gpcp.html)
314 [.gpcp.html](https://ps1.noaa.gov/data/gridded/data.gpcp.html)). The SST dataset is accessible at [https://ps1.noaa.gov/data/gridded/](https://ps1.noaa.gov/data/gridded/data.noaa.ersst.v5.html)
315 [data.noaa.ersst.v5.html](https://ps1.noaa.gov/data/gridded/data.noaa.ersst.v5.html). The CFSv2 simulations of model M1 are based on following
316 the experimental setup employed by Rajendran et al. (2021) and Singhai et al. (2023), while
317 the NCEP-CFSv2 retrospective runs used for verification purposes are generated by Saha et
318 al. (2010) and are available through NCEP at [https://www.ncdc.noaa.gov/data-access/](https://www.ncdc.noaa.gov/data-access/model-data/model-datasets/climate-forecast-system-version2-cfsv2)
319 [model-data/model-datasets/climate-forecast-system-version2-cfsv2](https://www.ncdc.noaa.gov/data-access/model-data/model-datasets/climate-forecast-system-version2-cfsv2).

References

320

321 Atger, F. (1999). The skill of ensemble prediction systems. *Monthly Weather Review*,
322 *127*(9), 1941–1953.

323 Cash, B. A., Barimalala, R., Kinter, J. L., Altshuler, E. L., Fennessy, M. J., Manganello,
324 J. V., ... Vitart, F. (2017). Sampling variability and the changing enso–monsoon
325 relationship. *Climate Dynamics*, *48*, 4071–4079.

326 Chakraborty, A., & Singhai, P. (2021). Asymmetric response of the Indian summer monsoon
327 to positive and negative phases of major tropical climate patterns. *Scientific reports*,
328 *11*(1), 1–13.

329 Charney, J. G., & Shukla, J. (1981). Predictability of monsoons. *Monsoon dynamics*,
330 99–110.

331 Chattopadhyay, R., Rao, S. A., Sabeerali, C., George, G., Rao, D. N., Dhakate, A., &
332 Salunke, K. (2016). Large-scale teleconnection patterns of Indian summer monsoon
333 as revealed by CFSv2 retrospective seasonal forecast runs. *International Journal of*
334 *Climatology*, *36*(9), 3297–3313.

335 Das, R. S., Rao, S. A., Pillai, P. A., Srivastava, A., Pradhan, M., & Ramu, D. A. (2022).
336 Why coupled general circulation models overestimate the ENSO and Indian summer
337 monsoon rainfall (ismr) relationship? *Climate Dynamics*, *59*(9-10), 2995–3011.

338 George, G., Rao, D. N., Sabeerali, C., Srivastava, A., & Rao, S. A. (2016). Indian summer
339 monsoon prediction and simulation in CFSv2 coupled model. *Atmospheric Science*
340 *Letters*, *17*(1), 57–64.

341 Gershunov, A., Schneider, N., & Barnett, T. (2001, June). Low-frequency modulation of
342 the ENSO–indian monsoon rainfall relationship: Signal or noise? *Journal of Climate*,
343 *14*(11), 2486–2492. Retrieved from [https://doi.org/10.1175/1520-0442\(2001\)](https://doi.org/10.1175/1520-0442(2001)014<2486:lfmote>2.0.co;2)
344 [014<2486:lfmote>2.0.co;2](https://doi.org/10.1175/1520-0442(2001)014<2486:lfmote>2.0.co;2) doi: 10.1175/1520-0442(2001)014<2486:lfmote>2.0.co;2

345 He, L., Zhou, T., & Chen, X. (2022). South asian summer rainfall from CMIP3 to CMIP6
346 models: biases and improvements. *Climate Dynamics*, 1–13.

347 Huang, B., Thorne, P. W., Banzon, V. F., Boyer, T., Chepurin, G., Lawrimore, J. H.,

- 348 ... Zhang, H.-M. (2017). NOAA extended reconstructed sea surface temperature
349 (ERSST), version 5. *NOAA National Centers for Environmental Information*, 30,
350 8179–8205.
- 351 Huffman, G. J., Adler, R. F., Bolvin, D. T., & Gu, G. (2009). Improving the global
352 precipitation record: GPCP version 2.1. *Geophysical Research Letters*, 36(17).
- 353 Kim, H.-M., Webster, P. J., Curry, J. A., & Toma, V. E. (2012). Asian summer monsoon
354 prediction in ECMWF System 4 and NCEP CFSv2 retrospective seasonal forecasts.
355 *Climate Dynamics*, 39, 2975–2991.
- 356 Krishnamurthy, V. (2018). Seasonal prediction of South Asian monsoon in CFSv2. *Climate*
357 *Dynamics*, 51(4), 1427–1448.
- 358 Kucharski, F., Bracco, A., Yoo, J., & Molteni, F. (2007). Low-frequency variability of the
359 Indian monsoon–ENSO relationship and the tropical Atlantic: The “weakening” of
360 the 1980s and 1990s. *Journal of Climate*, 20(16), 4255–4266.
- 361 Kucharski, F., Bracco, A., Yoo, J., & Molteni, F. (2008). Atlantic forced component of the
362 Indian monsoon interannual variability. *Geophysical Research Letters*, 35(4).
- 363 Leutbecher, M., & Palmer, T. N. (2008). Ensemble forecasting. *Journal of computational*
364 *physics*, 227(7), 3515–3539.
- 365 Molteni, F., Buizza, R., Palmer, T. N., & Petroliagis, T. (1996). The ECMWF ensem-
366 ble prediction system: Methodology and validation. *Quarterly journal of the royal*
367 *meteorological society*, 122(529), 73–119.
- 368 Palmer, T. N. (2000). Predicting uncertainty in forecasts of weather and climate. *Reports*
369 *on progress in Physics*, 63(2), 71.
- 370 Parthasarathy, B., Munot, A., & Kothawale, D. (1994). All-India monthly and seasonal
371 rainfall series: 1871–1993. *Theoretical and Applied Climatology*, 49(4), 217–224.
- 372 Pillai, P. A., Rao, S. A., Srivastava, A., Ramu, D., Pradhan, M., & Das, R. S. (2021).
373 Impact of the tropical Pacific SST biases on the simulation and prediction of indian
374 summer monsoon rainfall in CFSv2, ECMWF-System4, and NMME models. *Climate*
375 *Dynamics*, 56, 1699–1715.

- 376 Rajeevan, M., Bhate, J., Kale, J., & Lal, B. (2006). High resolution daily gridded rainfall
377 data for the Indian region: Analysis of break and active monsoon spells. *Current*
378 *Science*, 296–306.
- 379 Rajendran, K., Surendran, S., Varghese, S. J., & Chakraborty, A. (2021). Do seasonal
380 forecasts of indian summer monsoon rainfall show better skill with February initial
381 conditions? *Current Science (00113891)*, 120(12).
- 382 Rajendran, K., Surendran, S., Varghese, S. J., & Sathyanath, A. (2022). Simulation of indian
383 summer monsoon rainfall, interannual variability and teleconnections: evaluation of
384 CMIP6 models. *Climate Dynamics*, 58(9-10), 2693–2723.
- 385 Ramu, D. A., Chowdary, J. S., Ramakrishna, S., & Kumar, O. (2018). Diversity in the
386 representation of large-scale circulation associated with enso-indian summer monsoon
387 teleconnections in CMIP5 models. *Theoretical and applied climatology*, 132, 465–478.
- 388 Rasmusson, E. M., & Carpenter, T. H. (1983). The relationship between eastern equato-
389 rial Pacific sea surface temperatures and rainfall over India and Sri Lanka. *Monthly*
390 *Weather Review*, 111(3), 517–528.
- 391 Sabeerali, C., Ajayamohan, R., Bangalath, H. K., & Chen, N. (2019). Atlantic Zonal
392 Mode: An emerging source of Indian summer monsoon variability in a warming world.
393 *Geophysical Research Letters*, 46(8), 4460–4467.
- 394 Saha, S., Moorthi, S., Pan, H.-L., Wu, X., Wang, J., Nadiga, S., . . . others (2010). The ncep
395 climate forecast system reanalysis. *Bulletin of the American Meteorological Society*,
396 91(8), 1015–1058.
- 397 Saha, S., Moorthi, S., Wu, X., Wang, J., Nadiga, S., Tripp, P., . . . others (2014). The
398 NCEP climate forecast system version 2. *Journal of climate*, 27(6), 2185–2208.
- 399 Shukla, J., & Wallace, J. (1983). Numerical simulation of the atmospheric response to
400 equatorial Pacific sea surface temperature anomalies. *Journal of the Atmospheric*
401 *Sciences*, 40(7), 1613–1630.
- 402 Shukla, R. P., & Huang, B. (2016). Mean state and interannual variability of the indian
403 summer monsoon simulation by NCEP CFSv2. *Climate Dynamics*, 46, 3845–3864.

- 404 Singh, B., Cash, B., & Kinter III, J. L. (2019). Indian summer monsoon variability forecasts
405 in the North American multimodel ensemble. *Climate dynamics*, *53*(12), 7321–7334.
- 406 Singhai, P., Chakraborty, A., Rajendran, K., & Surendran, S. (2023). Why is the in-
407 dian summer monsoon in CFSv2 hypersensitive to moisture exchange with the Pacific
408 Ocean? *Climate Dynamics*, 1–17.
- 409 Tippett, M. K., Trenary, L., DelSole, T., Pegion, K., & L'Heureux, M. L. (2018). Sources
410 of bias in the monthly cfsv2 forecast climatology. *Journal of Applied Meteorology and
411 Climatology*, *57*(5), 1111–1122.
- 412 Weisheimer, A., Palmer, T., & Doblas-Reyes, F. (2011). Assessment of representations of
413 model uncertainty in monthly and seasonal forecast ensembles. *Geophysical Research
414 Letters*, *38*(16).